Low Temperature Physics/Fizika Nizkikh Temperatur, 2013, v. 39, No. 9, pp. 986–991

Spin waves in the *B*-phase of superfluid ^{3}He in confined cylindrical geometry

O.W.B. Benningshof and R. Jochemsen

Kamerlingh Onnes Laboratory, Leiden University, P.O. Box 9504, 2300 RA Leiden, the Netherlands
E-mail: Jochemsen@Physics.LeidenUniv.nl

Received March 4, 2013

We describe experiments on superfluid ^{3}He in a cylinder of 1 mm in diameter. This geometry causes the preferred orientation of the **n**-vector in the superfluid *B*-phase to be locally different, resulting in a curved configuration across the sample. Exclusive to our experiment is the observation that we succeeded in obtaining a texture which is metastable and unchanged in our pressure and temperature ranges, most likely because the experiment is performed at low pressures and low magnetic fields. As this texture can be considered as a potential for spin waves, we had the unique opportunity to study spin waves for several pressures in exactly the same texture. Our geometry causes this texture potential to be nearly quadratic, allowing an analytic solution of the theory which can be compared to our experimental results. As predicted we find the intensities of all spin wave modes more or less equal. Increasing the pressure shows a gradual increase in the number of spin wave modes in our cell. Finally we were able to cause a transition from the metastable to the predicted stable texture, concluding unexpectedly that the metastable texture is realized if the growing (or cooling) speed is sufficiently slow.

PACS: *67.30.he* Textures and vortices;
67.30.hj Spin dynamics;
67.30.ht Restricted geometries.

Keywords: superfluid *B*-phase, metastable texture, ^{3}He.

Introduction

The superfluid *B*-phase of liquid ^{3}He is characterized by the relative broken symmetry of the spin angular momentum (**S**) and orbital angular momentum (**L**) of the Cooper pairs, of which the order parameter is proportional with the spin-orbit rotation matrix $\mathbf{R}(\mathbf{n},\theta)$ [1]. The angle θ between the two vectors is fixed, and equals the Leggett angle $\theta_L \approx 104°$. The normal to the plane formed by **L** and **S** is named the rotation axis **n**, which is a convenient vector quantity to describe any orientation effects in the *B*-phase. The bulk superfluid *B*-phase is isotropic, consequently the **n**-vector will not have any preferred orientation. However, walls and magnetic fields will introduce a preferred orientation of the **n**-vector.

In confined geometries and in a magnetic field the orientation of the **n**-vector will be locally different, meaning that the **n**-vector is bent over the sample. The bending is of the typical size of the magnetic healing length ξ_H, and forms a potential for spin waves. These spin waves can be detected by transverse Nuclear Magnetic Resonance (NMR) experiments, and are observed as satellite peaks in the absorption spectrum. In general the differential equations concerning these spin dynamics are not trivial to solve for a given geometry. However, for the parallel-plate and cylindrical geometries the differential equation, to a certain extent, can be solved [2].

In the case of slab geometry (separation of the plates $L \leq \xi_H$) and $\mathbf{B}_0$ parallel to the plates, transverse NMR experiments did detect spin waves [3]. Here the spacing between the spin wave modes (NMR resonances) was more or less constant, and the intensity dropped as a function of k^{-1}, where k is the spin wave mode. This is in good agreement (at least to first order) with the solution of the differential equation for this geometry [4,5].

The spin wave experiments performed in cylindrical geometries (R is few times ξ_H) do show a decrease of intensity with increasing k as well, see for example Hakonen *et al*. [6]. The experiments, concerning this geometry, could be explained by numerical calculations [7]. Here the configuration of the texture (which forms the effective potential) was determined by minimizing the appropriate free energy and solving the resulting Euler–Lagrange equations. The magnetic healing length decreases as function of temperature, consequently the effective potential for the spin waves is temperature dependent. Normally, this is considered the dominating temperature effect for spin waves in the cylindrical geometry [8].

Here, we present that we have been able to grow a **n**-texture, which is meta-stable and does not change below a certain temperature. Not only do we create this way a temperature independent potential, but this potential is also close to a quadratic one, for which the corresponding differential equation can be solved analytically.

2. Theory

The orientation of the **n**-vector in superfluid ^{3}He–B is determined by the magnetic field in the bulk liquid and by the proximity to the wall of the cell. The strength of the magnetic field, which is the static magnetic field to perform NMR, is around 15 mT, for which the superfluid is in the high field limit ($B >> 3$ mT). In this case the most important orientation energies are: the bulk-field free energy F_{BH}, the bulk-bending free energy F_{BB} and the surface-field free energy F_{SH}. The total free energy to be minimized is

$$F = F_{BH} + F_{BB} + F_{SH}. \qquad (1)$$

The bulk-field energy is minimized when the **n**-vector is aligned with the magnetic field [4]. In the case that $\mathbf{B}_0$ is perpendicular to the normal to the wall $(\hat{\mathbf{s}})$, as in the case of our experiments, it is shown [4] that F_{SH} is minimized when **n** makes an angle $\beta = \arccos(1/\sqrt{5}) \simeq 64.5°$ with respect to both $\hat{\mathbf{s}}$ and $\mathbf{B}_0$. However, the change in the local orientation can only be continuous, since fast changes (discontinuities) of the order parameter will be energetically unfavorable. One accomplishes a smoothing of the spatial variations over a finite distance, if F_{BB} is expressed as an invariant combination of the gradients of the order parameter [4,9]. The superfluid takes the configuration which minimizes the total free energy over the whole sample. This results in a continuous change of the orientation of the **n**-vector over the whole sample, and this configuration is called the **n**-texture [9].

For the case of an axial magnetic field and a cylindrical geometry with radius $R \gg \xi_H$, one can calculate that the energetically most favorable configuration of the **n**-texture is the flare-out configuration, as calculated by Smith, Brinkman and Engelsberg [4]. Here we expect that the **n**-vector has an angle with $\mathbf{B}_0$ and $\hat{\mathbf{s}}$ of $\arccos(1\sqrt{5})$ at the wall ($r = R$) of the cylinder and that it will align itself over a typical length ξ_H parallel to the z-axis (and the magnetic field) in the center of the cylinder. These two boundary conditions change the **n**-vector orientation in a spiral-like configuration, which can be parameterized by

$$\hat{\mathbf{n}} = \sin\beta\cos\alpha\hat{\mathbf{r}} + \sin\beta\sin\alpha\hat{\mathbf{j}} + \cos\beta\hat{\mathbf{z}}, \qquad (2)$$

in cylindrical coordinates. The angles α and β are functions of r only, and their behavior is intensely studied [7,10,11]. The angle α is hardly r dependent and is in practice close to $\alpha \approx \pi/3$. The angle β between the **n**-vector and magnetic field varies smoothly over the sample between values fixed by the boundary conditions. Both radial dependencies are experimentally confirmed by Spencer *et al*. [12,13].

The magnetic healing length is proportional to $\sim\sqrt{1-T/T_c}/B$ [8,11,13], meaning that it increases during cooling, and the flare-out texture gradually grows in a spiral way to the center. The growing should be able to continue as long as the boundary conditions can be fulfilled, meaning that the flare-out texture will grow as long as it is the most energetically favorable configuration. Simulations [11] till ratios of $\xi_H/R > 0.5$ support this idea of growing. Quantitative calculations for higher ratios seem to be tough. One may assume that the most extreme form of the flare-out configuration would be the gradual change of the **n**-vector connecting the two boundary conditions. Not clear is how this energetically compares to other textures. Actually, because of complexity of the calculations, it is not clear at all how transitions to other textures should occur when $\xi_H \geq R$. The qualitative answer for the limit $\xi_H \gg R$ is clear. The texture should be completely uniform [7], and β should have an angle of $\arccos(1/\sqrt{5})$, as directed by the boundary condition at the wall.

To study any textural transitions we consider a cylindrical geometry with a diameter of 1 mm. Converting back the magnetic healing length as found in literature [8,11,13] to our pressures (0–6 bar) and magnetic field (15 mT), it is 5 to 10 times longer than the radius of the cylinder at 0.7 T/T_c. If one starts cooling all textures initially started to grow in the flare-our configuration. The growing continues till temperatures around 0.7 T/T_c. Lower temperatures leave the texture unchanged, so a textural transition is not observed. It is believed that this flare-out configuration is formed where the two boundary condition are directly connected, or with other words, the **n**-vector is gradually changed over the whole range of the sample. This texture is stable, but is not expected on energetic grounds, for which we consider this a metastable texture. The reason may be that a transition corresponds with sharp jumps in the **n**-texture, which will definitely be discouraged by the bulk-bending free energy. However, the bending of the **n**-vector will act as an attractive potential for spin waves, resulting in a temperature independent potential for various pressures for temperatures below 0.7 T/T_c.

For the flare-out texture in a long circular cylinder with the axis aligned with the magnetic field one can formulate the differential equation concerning the spin dynamics. In the transverse case, relevant for our transverse NMR experiments, it is given by [2,7,10,11,14]

$$(-\bar{K} + \bar{K}' \mid R^L_{+r} \mid^2)\xi_D^2\left[\frac{1}{r}\frac{d}{dr}\left(r\frac{d}{dr}\right)\right]\psi_{+,k} -$$

$$-(1-\frac{1}{2}\sin^2\beta)\psi_{+,k} = E_{+,k}\psi_{+,k}. \qquad (3)$$

The first term can be seen as the kinetic part. Here $\bar{K}$ and $\bar{K}'$ are dimensionless parameters which equal 8/5 and 4/5, respectively, if calculated in the weak-coupling Ginzburg–Landau [15] approximation. R^L_{+r} are the transverse components of the spin-orbit rotation matrix, and ξ_D is the dipole coherence length. The second part in Eq. (3) is the potential part, which is formed by the relevant transverse components of Eq. (2). The eigenvalues are given by the following equation

$$\omega^2_{+,k} - \omega_{+,k}\omega_L - \Omega^2_B = E_{+,k}\Omega^2_B, \tag{4}$$

where $\omega_{+,k}$ corresponds with the frequency of the kth spin wave mode, ω_L is the Larmor frequency and Ω_B the longitudinal NMR frequency of the B-phase.

In general the differential Eq. (3) is not trivial to solve, especially in combination with a temperature dependent potential. However, in our case we have a temperature independent potential, and moreover, our potential only differs maximally 6.5% if the term $\frac{1}{2}\sin^2\beta$ is approximated by a quadratic dependency in r. As the potentials are very alike, it is convenient to compare the data with the results from a quadratic potential, for which the differential equation is analytically solvable. It reduces to the Schrödinger equation for the two dimensional harmonic oscillator, for which the eigenvalues are given by

$$E_{+,k} = -1 + 2\sqrt{\left(\bar{K} - \frac{1}{2}\bar{K}'\right)}\frac{\xi_D}{\Re}(k+1), \tag{5}$$

where $\Re$ is the measure of curvature of the potential. Only s-wave states couple to the homogeneous rf field, or with other words: only the $l = 0$ modes have nonvanishing intensities in experiments using uniform rf fields [7]. Consequently, only the even k modes couple to the corresponding NMR frequencies. The eigenvalues have constant separation and, as this is a two dimensional system in a quadratic potential (density of states is constant), the intensities should all be equal. Interesting is that in the Ginzburg–Landau regime [2], the eigenvalues are pressure dependent, as ξ_D changes as function of pressure, which tunes it between 32 μm (zero pressure) and 7 μm (melting pressure). As the energy landscape (potential energy) for all pressures is the same, while the level spacing of the eigenvalues decreases with increasing pressure, the amount of spin wave modes in the cylinder should grow.

In reality ξ_D does also change with temperature [8], but this dependency is weak, certainly compared to the temperature dependency in Ω_B [16], as it is proportional with $\Delta(T)^2/\chi_B$. The temperature behavior of the energy gap $\Delta(T)$ and the susceptibility χ_B for the superfluid B-phase are both experimentally and theoretically known [17–19], meaning that our system, including the growing of spin wave modes, is in theory completely known.

3. Cell

A schematic drawing of the final cell is shown in Fig. 1. The cell is constructed on a block of copper, which fits on the experimental space of the nuclear stage and is 10 mm thick. In this way the cell with all the various components could be assembled outside the cryostat, including the magnet, and could easily be screwed on the nuclear stage. The cell itself mainly consists out of silver and polyetherimide (PEI).

The silver piece sliced into the copper block, and was rigidly fixed with additional bolts. One should be sure that copper and silver pieces are squeezed sufficiently against each other, to prevent extra impedance for the thermal conduction. The silver piece itself, which has good thermal conducting properties at low temperatures [20], should cool the ^{3}He to the temperatures of the nuclear stage. Silver is preferred over copper, despite the fact that it has a lower thermal conductance, because its properties are more favorable in the presence of a magnetic field. However, the interfacial thermal resistance, better known as the Kapitza resistance R_K, between the liquid ^{3}He and the silver becomes rather high at low temperatures. The amount of vibrations (phonons) is strongly decreased at low temperatures and in combination with the mismatch at the interface (low scatter probability) this gives a high Kapitza resistance. The temperature difference across such interface is given by

$$\Delta T = \frac{R_K \dot{Q}}{A}, \tag{6}$$

where $\dot{Q}$ is the heat flow and A the surface area of the interface. In the case of an interface between ^{3}He and silver the Kapitza resistance at 2 mK is $R_K = 10^5$ m^2·K·W^{-1} [20]. To prevent the interface of becoming the highest impedance of the heat transport, the area should be made sufficiently large. This is accomplished by a silver sinter pressed on the silver piece. Here the sinter works as a sponge in the ^{3}He liquid and has an enormous surface area. The silver sinter was 0.5 mm thick and had an effective area

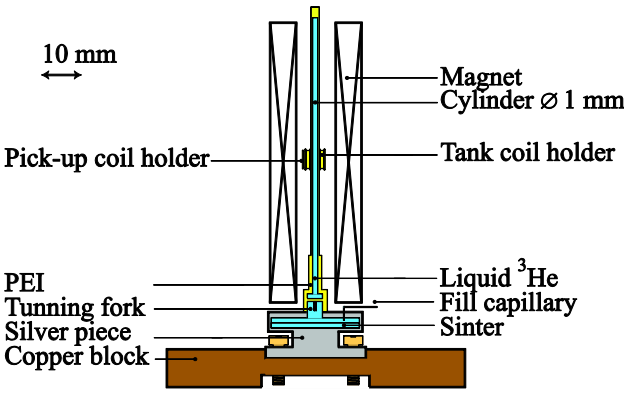

Fig. 1. (Color online) Cross section of the experimental cell.

of 25 m^2, which gives a $\dot{Q}/\Delta T$ ratio of $2.5{\cdot}10^{-4}$ $W{\cdot}K^{-1}$. This is one order of magnitude better than the heat transport through helium in the cylinder, as we will see later, and made this interface not a limitation in the cool down process.

The part of the cell which fits into the magnet should be made of a non-metallic material. Otherwise it would lead to significant losses like eddy currents, which is bad for temperature stability and NMR measurements. For this purpose this part of the cell is mainly made out of polyetherimide. PEI is a plastic which is easily to machine and has proven to be suitable to work with at low temperatures, meaning it does not crack after multiple cool downs. The disadvantage of working with PEI, whose molecular structure per unit polymer is given by $C_{37}H_{24}O_6N_2$, is the quantity of hydrogen atoms in it. The gyromagnetic ratio γ of hydrogen is relatively close to the one of ^{3}He (they differ approximately by a factor of ~ 1.31) and because the T_2 of hydrogen in the polymer is short, the tail of the NMR absorption is visible at the resonance frequency of ^{3}He. From this point of view it is more desirable to work with quartz glass (SiO_2), it is also a nonmetal and has not a net nuclear spin. However, the fabrication and machining of quartz glass cylinders is much more complicated. Together with the fact that several cell's needed to be constructed to find the optimal results for cooling the liquid, SNR of the NMR experiments, fiber gluing, etc., made it more convenient to construct the cell out of PEI.

The experiment is performed in a circular cylinder made of PEI, which axis is aligned with the static magnetic field of the NMR. The total length is 70 mm and 1 mm in diameter. The read out is performed with a weakly coupled transformer technique [22], where the rf-coil is positioned in the middle of the cylinder.

4. Results

Measurements are performed between zero and 6 bar, and till temperatures below 300 μK. A typical sequence of NMR spectra at different temperatures is plotted in Fig. 2. Here the measurement is performed at 6 bar, and the temperature sweep is between 0.57 mK and 1.56 mK (transition temperature). Above T_c the resonance frequency occurs at the Larmor frequency. Directly below T_c, the liquid has undergone the phase transition to the superfluid *B*-phase, and the growing of the flare-out configuration is observed. The absorption spectrum has become wider, caused by the radial changes in the orientation of the **n**-vector in the cylinder.

The texture gets stuck around 1 mK, and from this point it forms a constant potential. Also around this temperature the spin waves modes become visible, as the separation between the modes is enough to distinguish each mode. The spin wave absorption lines are more or less equally separated, but more importantly they have approximately the same intensities. In total 5 spin wave modes become

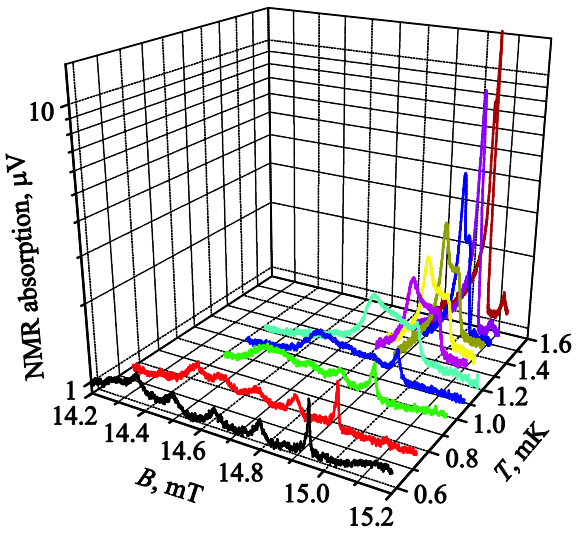

Fig. 2. (Color online) NMR absorption scans of helium in a cylinder with a radius of 0.5 mm at 6 bar for various temperatures. The absorption is expressed in voltage μV, which is the signal measured with the pick-up coil. The temperature range is between 0.57 mK and T_c (1.56 mK). At and above the transition temperature the absorption peak is at the Larmor frequency. At lower temperatures the resonance frequency shows a shift due to texture effects. At even lower temperatures, $T/T_c < 0.7$, several spin waves modes become visible.

clearly visible at the lowest temperatures, which is expected at this pressure according to Eq. (5). The separation between the modes does increase as Ω_B increases by decreasing temperature [3]. Below 0.3 T/T_c hardly any temperature dependency is observed, as the susceptibility and energy gap are almost saturated. This texture seems stable for the whole temperature range (at least till 100 μK), and no textural transition is noticed.

The NMR spectrum of the spin wave modes at several different pressures obtained at the lowest achievable temperatures ($T < 0.3\ T_c$) are shown in Fig. 3. No noticeable temperature effects are expected below 0.3 T_c, so the data can be compared with the results of the theory at zero temperature (Eqs. (4) and (5)). The zero temperature theory predicts the frequencies of the spin wave with only the pressure as a variable. The longitudinal NMR frequency Ω_B of the *B*-phase is very well known as a function of pressure [3,16]. The most important approximation is the replacement of the real texture potential in Eq. (3) by a quadratic one, which allowed the analytical solution of the spin wave frequencies as given in Eq. (5). The theoretical frequencies for the various spin wave modes are shown in Fig. 3 as colored dotted-solid curves. The black (*1*) and red (*2*) curve represents the $k = 0$ and $k = 2$ mode, respectively. Both exists at all pressures. The sequence green (*3*), blue (*4*) and cyan (*5*) represent the $k = 4$, 6 and 8 modes, which only exist at increasing pressure, allowing 5 modes at a pressure of 6 bar.

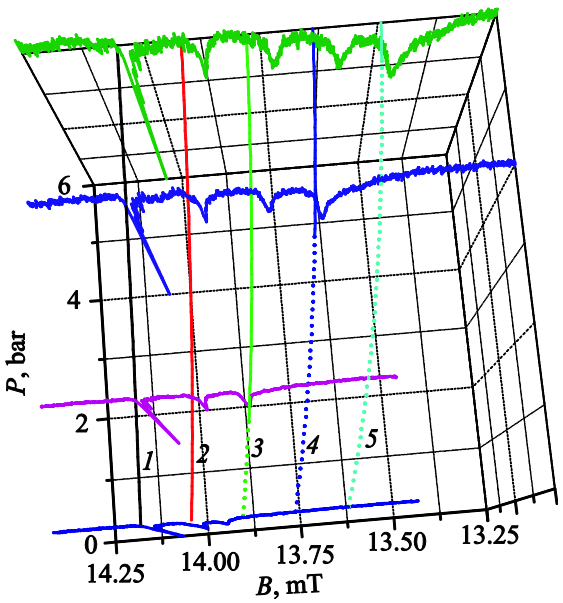

Fig. 3. (Color online) Spin wave absorption peaks as a function of magnetic field at pressures of 0, 1.5, 4 and 6 bar. Each absorption line is obtained at a temperature below 0.3 T/T_c. The absorption is expressed in arbitrary units. The longest peak corresponds with the mode $k = 0$ in Eq. (5), the neighboring peak corresponds to the mode $k = 2$, and so on. The (more or less vertical) curves represent the theoretically predicted spin wave frequencies for the various modes at zero temperature. The black (*1*), red (*2*), green (*3*), blue (*4*) and cyan (*5*) dotted/solid curves correspond with the mode 0, 2, 4, 6 and 8, respectively. All curves are plotted for increasing pressures (started from 0 pressure), but the curve is dashed when the mode is predicted not to exist, and it becomes a solid curve when theory predicts the mode to exist.

The measurements are in good qualitative agreement with the theory, both the frequencies of the modes and the number of existing spin modes at a certain pressure. The theory predicts a somewhat smaller spacing between the frequencies of the spin modes, which can be explained by the fact that the real potential is a bit steeper than the quadratic potential, except close to the cell wall [21]. The number of observed spin modes at each pressure is exactly as predicted by theory, with one exception: for zero pressure one would expect 2 spin wave modes, while 3 modes can be distinguished in the NMR absorption line.

5. Discussion

The flare-out configuration for the texture is not the expected minimum-energy state for the ratios of R/ξ_H in our experiment. However, it seems to be a stable state and once the liquid has been cooled to the superfluid state in this configuration no transition to an other textural configuration is observed. We guess that the forming of this meta-stable texture occurs at sufficiently slow cooling. Once grown far enough in the flare-out configuration this state is meta-stable, as the threshold to jump to an other textural configuration is too high.

If one would cool down more rapidly, the magnetic healing length ξ_H would grow and oversize the radial dimension of the system much faster than in normal procedure. At the moment the superfluid is formed, the $\hat{\mathbf{n}}$-vector is not given enough the time to grow smoothly into the flare-out configuration. This condition will favor the creation of the forming of the uniform-texture. To cool as fast as possible with our setup, the liquid was pre-cooled to the lowest temperatures, and than locally heated to the normal state by a rf-pulse. While the rest of the system is still cold the heat only needs to be removed locally, which should make the cooling much faster than in any other method available. Enough heat could be produced with a pulse in the rf-coil, the absorption was enough to overcome locally the energy gap, and it turns out the superfluid cools into another textural state. This is depicted in Fig. 4. The black (*1*) absorption line shows the usual stable situation at 6 bar (around 300 μK) with the 5 spin wave modes. After the heat pulse, the resonance frequency is at the Larmor frequency, as shown by the green (*3*) absorption line, indicating that the liquid is in the normal state. The locally heated liquid then starts to cool and the absorption peak moves uniformly to the left and becomes wider as the liquid becomes superfluid. The red (*2*) curve in Fig. 4 shows the equilibrium result, when the liquid is cooled back to 300 μK. The spin wave modes have disappeared, and the NMR absorption signal only shows a single peak, indicat-

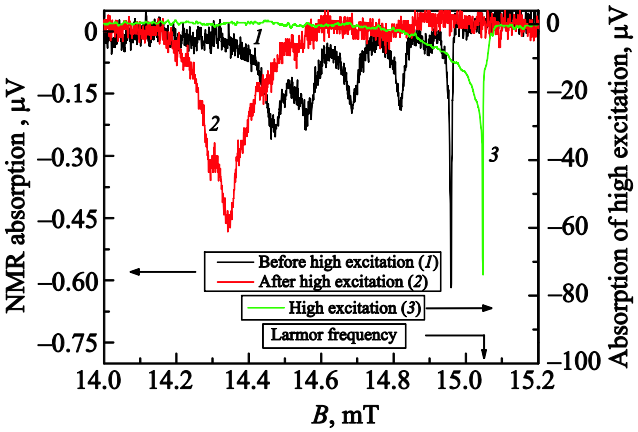

Fig. 4. (Color online) Local heating of the superfluid with NMR. The black (*1*) and red (*2*) curves show the absorption spectrum of 6 bar at 300 μK before and after heating the sample, respectively. The corresponding values of both absorption curves are put on the left *y*-axis. The green (*3*) curve corresponds with the absorption curve while heating the sample, absorption values are put on the right *y*-axis. Here the values are 2 orders of magnitude higher, so enough energy is dissipated to locally warm up the liquid to the normal state, as is indicated by a jump of the peak to the Larmor frequency. After the local heating, the texture is changed from flare-out to uniform configuration.

ing that the superfluid is in an uniform texture. This is the energetically expected uniform texture, where the center of the peak corresponds with $\beta \arccos(1/\sqrt{5})$, as is directed by the boundary condition at the wall.

1. A.J. Leggett, *Rev. Mod. Phys*. **47**, 331 (1975).
2. D. Vollhardt and P. Wölfle, *The Superfluid Phases of Helium 3*, Taylor and Francis, London (1990).
3. D.D. Osheroff, *Physica B+C* **90**, 20 (1977).
4. H. Smith, W.F. Brinkman, and S. Engelsberg, *Phys. Rev. B* **15**, 199 (1977).
5. Y.R. Lin-Liu and K. Maki, *Phys. Rev. B* **18**, 4724 (1978).
6. P.J. Hakonen, O.T. Ikkala, S.T. Islander, O.V. Lounasmaa, and G.E. Volovik, *J. Low Temp. Phys*. **53**, 425 (1983).
7. K.W. Jacobsen and H. Smith, *J. Low Temp. Phys*. **52**, 527 (1983).
8. P.J. Hakonen, M. Krusius, M.M. Salomaa, R.H. Salmelin, J.T. Simola, A.D. Gongadze, G.E. Vachnadze, and G.A. Kharadze, *J. Low Temp. Phys*. **76**, 225 (1989).
9. P.G. De Gennes, *Phys. Lett. A* **44**, 271 (1973).
10. P.J. Hakonen and G.E. Volovik, *J. Phys. C* **15**, L1277 (1982).
11. K. Maki and M. Nakahara, *Phys. Rev. B* **27**, 4181 (1983).
12. G.F. Spencer and G.G. Ihas, *Phys. Rev. Lett*. **48**, 1118 (1982).
13. G.F. Spencer and G.G. Ihas, *J. Low Temp. Phys*. **77**, 61 (1989).
14. S. Theodorakis and A.L. Fetter, *J. Low Temp. Phys*. **52**, 559 (1983).
15. P. Wölfle, *Phys. Lett. A* **47**, 224 (1974).
16. A.I. Ahonen, M. Krusius, and M.A. Paalanen, *J. Low Temp. Phys*. **25**, 421 (1976).
17. B. Mühlschlegel, *Z. Phys*. **155**, 313 (1959).
18. A.I. Ahonen, T.A. Alvesalo, M.T. Haikala, M. Krusius, and M.A. Paalanen, *Phys. Lett. A* **51**, 279 (1975).
19. L.R. Corruccini and D.D. Osheroff, *Phys. Rev. B* **17**, 126 (1978).
20. F. Pobell, *Matters and Methods at Low Temperatures*, Springer-Verslag, Berlin (1992).
21. O.W.B. Benningshof, *Superfluid Helium-3 in Cylindrical Restricted Geometries: A Study with Low Frequency NMR, Thesis Leiden University* (2011).
22. O.W.B. Benningshof, D.H. Nguyen, and R. Jochemsen, *J. Phys: Conf. Ser*. **150**, 012004 (2009).